**Paper**
Int'l J. of Aeronautical & Space Sci. 18(3), 474–484 (2017)
DOI: http://dx.doi.org/10.5139/IJASS.2017.18.3.474

IJASS
International Journal of Aeronautical and Space Sciences

# Application of Artificial Neural Networks to Predict Dynamic Responses of Wing Structures due to Atmospheric Turbulence

**Anh Tuan Nguyen***

*Faculty of Aerospace Engineering, Le Quy Don Technical University, Hanoi 122314, Vietnam*
*Department of Aerospace Engineering, KAIST, Daejeon 34141, Republic of Korea*

**Jae-Hung Han****

*Department of Aerospace Engineering, KAIST, Daejeon 34141, Republic of Korea*

**Anh Tu Nguyen*****

*Department of Automatics and Computer Systems, National Research Tomsk Polytechnic University, Tomsk 634050, Russian Federation*

## Abstract

This paper studies the applicability of an efficient numerical model based on artificial neural networks (ANNs) to predict the dynamic responses of the wing structure of an airplane due to atmospheric turbulence in the time domain. The turbulence velocity is given in the form of a stationary Gaussian random process with the von Karman power spectral density. The wing structure is modeled by a classical beam considering bending and torsional deformations. An unsteady vortex-lattice method is applied to estimate the aerodynamic pressure distribution on the wing surface. Initially, the trim condition is obtained, then structural dynamic responses are computed. The numerical solution of the wing structure's responses to a random turbulence profile is used as a training data for the ANN. The current ANN is a three-layer network with the output fed back to the input layer through delays. The results from this study have validated the proposed low-cost ANN model for the predictions of dynamic responses of wing structures due to atmospheric turbulence. The accuracy of the predicted results by the ANN was discussed. The paper indicated that predictions for the bending moments are more accurate than those for the torsional moments of the wing structure.

**Key words:** Atmospheric turbulence, Artificial neural network, Gust response, Unsteady vortex-lattice method

## 1. Introduction

Atmospheric turbulence has been of great importance since the earliest days of aeronautical science [1,2]. The occurrence of atmospheric turbulence could be one of major obstacles to the success of aircraft performance. Estimating loads arising from atmospheric gusts is a classical problem that has been addressed in the requirements of Federal Aviation Regulations Part 25 (FAR 25) [3] and Certification Specifications Part 25 (CS 25) [4] for the large airplane category. Turbulence models with the Dryden or the von Karman forms [5] of the power spectral density (PSD) are frequently used to evaluate the performance or dynamic loads of airplanes during flight. Based on several assumptions, such as stationarity and Gaussian distribution, atmospheric turbulence can be generated in the time domain in the form of a random process [6,7]. From time-domain simulation results, various effects of atmospheric turbulence on the flight dynamic and structural characteristics of airplanes may be clarified.

For the simulations of structural dynamic responses while



* Assistant Lecturer
** Professor, Corresponding author: jaehunghan@kaist.ac.kr
*** Ph. D Student

Received: January 4, 2017 Revised: August 23, 2017 Accepted: September 10, 2017


http://ijass.org pISSN: 2093-274x eISSN: 2093-2480

encountering gusts, several aerodynamic models with the different levels of fidelity and efficiency have been utilized. For example, Kanda and Dowell [8] used a simple low-order two-dimensional model based on the potential flow theory with the inclusion of the Wagner and the Kussner functions for the effect of aerodynamic unsteadiness. On the other hand, higher-order methods, such as the doublet-lattice method, the unsteady vortex-lattice method, and the computational fluid dynamics (CFD) method have been employed by Khodaparast and Cooper [9], Wang et al. [10], and Raveh [11], respectively. Amongst these, the doublet-lattice method is a frequency-domain method with the applicability restricted to only linear aerodynamic problems [12]. To obtain time-domain solutions by this method, approximation techniques, such as those based on rational functions [13], must be used. In general, aerodynamic unsteadiness is important for the estimations of dynamic gust responses. When unsteady aerodynamics is considered, aerodynamic loads are not only dependent on the current flight state, but also on the flow history. Therefore, the computational cost may increase dramatically, especially when gust responses during a long duration of flight time are required to be determined. Using low-order aerodynamic methods such as that by Kanda and Dowell [8], the computational time could be reduced; however, this type of method may not have good fidelity while dealing with a three-dimensional problem.

On the basis of the above-mentioned studies, it is necessary to develop a computational method with high fidelity and modest computational effort to estimate the dynamic loads of airplane structures due to atmospheric turbulence. Recently, the concept of artificial neural network (ANN) has become popular in many fields, including aerospace engineering [14,15]. ANNs are built to mimic the way a biological brain solves problems by connecting large clusters of neurons. Regarding aeroelastic analyses, ANNs have been applied for the development of reduced-order models to predict the behaviors of structural dynamic responses in different conditions, such as flutter and limit cycle oscillations [16,17]. The application of ANNs to predict the dynamic responses of aircraft wing structures due to random atmospheric turbulence will be introduced for the first time in this paper. For this purpose, a three-layer ANN is developed and trained. After the training process, the prediction results of wing structural responses while encountering atmospheric turbulence by the ANN are validated against numerical solutions from structural dynamic equations for various different cases. The turbulence velocity is generated in the form of a stationary Gaussian random process that has the PSD given by the von Karman equation. The nonlinear unsteady vortex-lattice method (UVLM) and the classical beam theory are respectively applied for aerodynamic and structural problems. Before calculating dynamic responses due to atmospheric turbulence, the trim condition is obtained by an iterative method.

## 2. Material and Methods

### 2.1 Atmospheric Turbulence Model

Alike other studies by Beal [6], and Gao and Gu [7], the velocity of atmospheric turbulence is assumed to take the form of a stationary Gaussian random process, whose statistic characteristics do not change over time. Moreover, the effect of the vertical velocity component dominates those of the longitudinal and lateral components. Therefore, in this study, only the vertical turbulence velocity is considered, which is similar to the approach used in the literatures [8–10]. The turbulence model has the von Karman form with the PSD $\Phi$ given as [5]

$$\Phi(\omega) = \sigma_w^{\,2} \frac{L_s}{\pi V} \frac{1+\frac{8}{3}\left(1.339 L_s \frac{\omega}{V}\right)^2}{\left[1+\left(1.339 L_s \frac{\omega}{V}\right)^2\right]^{11/6}}, \tag{1}$$

where the frequency $\omega$ is in rad/s, $\sigma_w$ is the root-mean-square (RMS) gust velocity, $L_s$ is the scale of turbulence, and $V$ is the

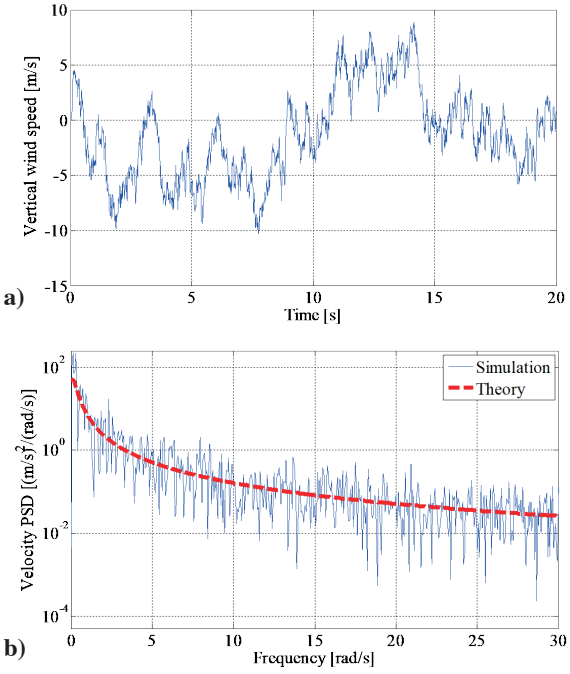


Fig. 1. Time history of simulated turbulence velocity (a); simulated and theoretical velocity PSDs (b)

flight speed. In this study, the scale of turbulence $L_s$ is equal to 762 m, according to FAR 25 [3]. The flight speed $V$ is set to 700 km/h that is typical for jet transport airplanes. The airplane is assumed to fly at an altitude of 8.0 km, corresponding to an air density of 0.5 kg/m$^3$.

To generate the turbulence velocity, a band-limited white noise is passed through an appropriate filter provided by Ly and Chan [18]. The simulated turbulence velocity with an RMS gust velocity $\sigma_w$ of 6.0 m/s is shown in Fig. 1 together with its PSD in comparison with a theoretical curve given by equation (1). Good agreement found in Fig. 1(b) has validated the method used to generate the atmospheric turbulence velocity in this study.

## 2.2 Structural Model

The present study employs the planform, as well as the mass and structural characteristics of a wing model given in the literature [19]. The wing has a span of 25.7 m, the planform area is 104.8 m$^2$, and the mass of the wing equals 22243.7 kg. The details about the wing structure and its geometry can be found in [19]. The wing is modeled by a classical (Euler-Bernoulli) beam undergoing bending and torsional deformations. Bending and torsional modes are obtained by a modal analysis using a finite-element method (FEM). These vibration modes will be coupled together later in the structural dynamic equations of the wing. The beam is divided into 50 two-node elements, and at each node we consider four degrees of freedom, including the vertical displacement $w$, rotation $\theta$ and their derivatives with respect to the coordinate along the beam axis. A more detailed description of the FEM can be found in [20]. The first four modes, including the two bending modes and two torsional modes of the right half of the wing, are illustrated in Fig. 2 together with their natural frequencies. Nguyen and Han [21] have indicated that for the current wing model, the inclusion of the first four modes are sufficient for the structural dynamics analysis. It is observed that the natural frequencies of the first two modes (1.86 Hz and 3.73 Hz) computed by the present FEM are close to the estimations by Bisplinghoff et al. [19] (2.04 Hz and 3.56 Hz).

## 2.3 Aerodynamic Model

The present study employs the nonlinear UVLM, which can provide the surface pressure difference between the upper and lower wing surfaces. Moreover, the wake is allowed to transport freely with the local velocity of the flow field; therefore, the effects of the wing-tip vortex and wake roll-up can be estimated precisely with this nonlinear aerodynamic model. The fundamental principles of the nonlinear UVLM could be found in the literatures [22–24]. According to these, the wing is discretized into a system of quadrilateral panels, on each we place a vortex ring. Moreover, each panel has a collocation point that is located at the centroid of the panel's corners. At the collocation points, we apply the no-

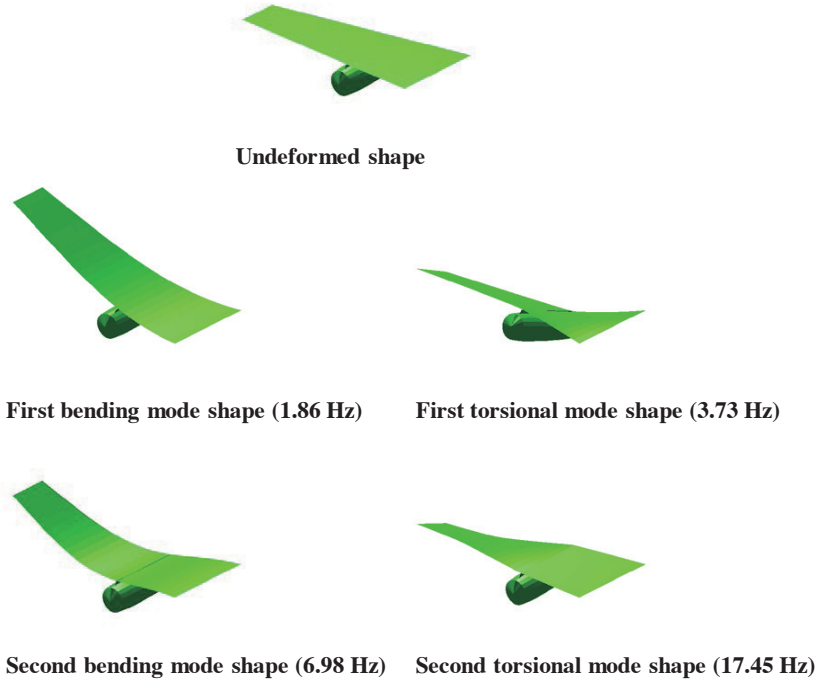


Fig. 2. The first four vibration modes of the wing

penetration boundary condition, which ensures that the normal component of the fluid velocity relative to the wing surface is zero. The Kutta condition is satisfied at the trailing edge of the wing; hence, all vortices are shed from this edge to form the free wake. The pressure difference between the lower and upper surfaces of the wing is calculated by the unsteady Bernoulli equation [22]. The panel mesh of the undeformed wing planform is shown in Fig. 3.

To validate the aerodynamic model, the unsteady lift coefficients $C_L$ of rectangular wings undergoing a sudden startup are computed and compared with those from the unsteady panel method combined with vortex-particle wakes by Willis et al. [25]. Here, we consider two wing models with the same chord length of 1.0 m, the aspect ratios $AR$ of these two wings are 4 and 8, and the free-stream velocity is 1.0 m/s. The good consistency between the results from the two methods (Fig. 4) has validated the present aerodynamic model.

The airplane model flies at 700 km/h at an altitude of 8 km, corresponding to a Mach number $M$ equal to 0.63. Therefore, the effect of compressibility must be included in the computation. For high-aspect-ratio wings, such as the current wing model, it is possible to apply the Prandtl-Glauert rule of the two-dimensional compressible flow [22]. Therefore, the pressure coefficient of a compressible flow $C_{pM}$ could be derived from the incompressible value $C_{p0}$ as follows:

$$C_{pM} = \frac{C_{p0}}{\sqrt{1-M^2}}. \tag{2}$$

## 2.4 Aeroelastic Coupling

To solve the aeroelastic problem, the wing structure is coupled with the nonlinear aerodynamic model. This paper supposes that a level flight at a constant speed is maintained, which is similar to assumptions in analyses of Zhang and Xiang [26] and Wang et al. [10]. Initially, the angle of attack and the deformed shape of the wing in the trim condition is obtained; and then under the trim condition, the wing structure is subject to various random atmospheric turbulence profiles.

### 2.4.1 Trim Search Method

The trim condition is found by an iterative method as shown in Fig. 5. Firstly, the aerodynamic pressure distribution on the wing surface $\{\Delta p\}$ is computed. Wing

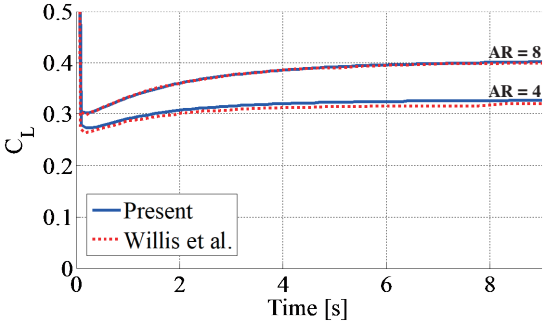


Fig. 4. Evaluations of lift coefficients $C_L$ of rectangular wings undergoing a sudden startup by the present aerodynamic model and by Willis et al. [25]

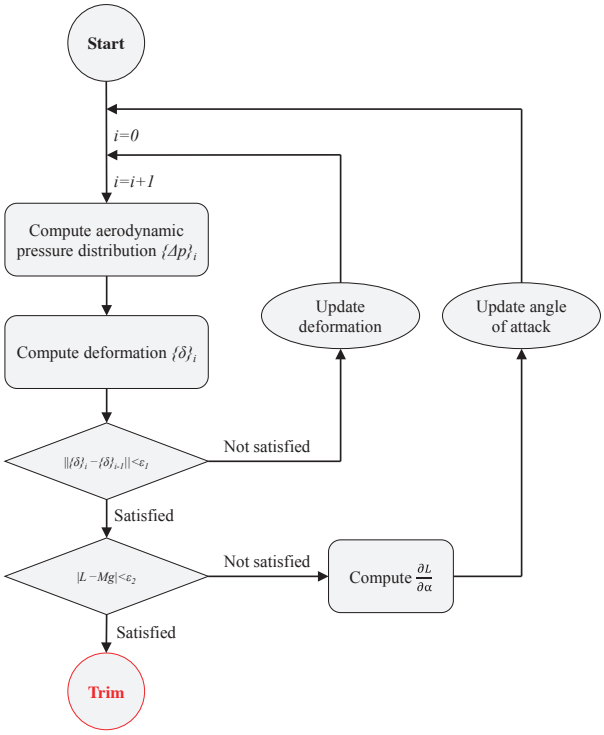


Fig. 5. Flowchart of the trim search method

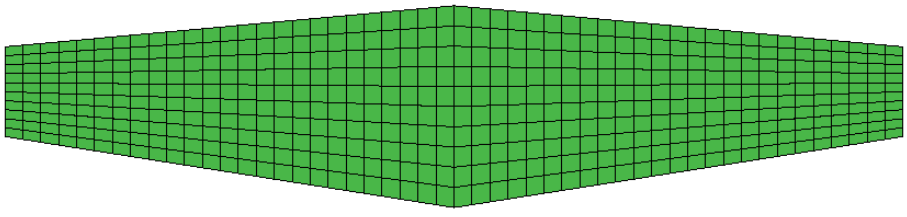

Fig. 3. Aerodynamic panel mesh

deformation $\{\delta\}$ due to the aerodynamic pressure and mass distributions is then calculated. Comparing the difference between the current deformation $\{\delta\}$i and the $(i\text{-}1)^{th}$ iteration of deformation $\{\delta\}_{i-1}$ with a prescribed error tolerance $\varepsilon_1$, we can check the convergence of the deformation solution. The deformation solution is obtained when the maximum error for bending is less than 1.0 cm (0.04% of the wing span), and that for torsion is less than 0.06 deg. Once the converged deformation has been achieved, lift is compared with the total weight of the airplane. The trim condition is satisfied when the difference between them is below $\varepsilon_2$=10 N (0.003% of the total weight). If this condition is not satisfied, the derivative of the lift L with respect to the angle of attack $\alpha$ is computed, and the increment of the angle of attack $\Delta\alpha$ is determined as

$$\Delta\alpha = \frac{Mg - L}{\partial L / \partial \alpha}, \tag{3}$$

where, $M$ is the total mass of the airplane, $g$ is the gravitational acceleration, and $L$ is the lift force.

After running the trim search program, the trim angle of attack was found to be 3.75 deg and the deformed shape of the wing in the trim condition is indicated in Fig. 6.

### 2.4.2 Structural Dynamic Equations

Figure 7 shows a wing-fixed coordinate system that has an origin located at the wing root. The $y$-axis of the coordinate system coincides with the elastic axis of the wing. $E$ and $C$ are the elastic center and the center of mass of a local wing cross section, respectively. The vertical displacement w at a location $(x,y)$ and time t due to dynamic responses can be expressed as

$$w(x,y,t) = \sum_{i=1}^{N_f} f_i(y) r_i(t) - x \sum_{j=1}^{N_\varphi} \varphi_j(y) s_j(t), \tag{4}$$

where $N_f$ and $N_\varphi$ are the numbers of bending and torsional modes. fi and $\varphi_j$ denote the shape functions of the ith bending mode and the jth torsional mode. The present study considers two bending modes and two torsional modes, which are illustrated in Fig. 2. $r_i$ and $s_j$ are time-dependent functions.

The kinematic energy $T$ due to the wing vibration is

$$T = \frac{1}{2} \int_0^{l/2} \left[ \int_{x_{L.E.}(y)}^{x_{T.E.}(y)} \rho(x,y) \left( \frac{\partial w(x,y,t)}{\partial t} \right)^2 dx \right] dy, \tag{5}$$

in which, $l$ is the wing span, $x_{L.E.}$ and $x_{T.E.}$ respectively represent the coordinates of the leading and trailing edges on the $x$-axis, and $\rho$ is the mass of a unit area of the wing planform. From equation (4) and the orthogonality of the mode shape functions [27], it follows that

$$T = \frac{1}{2} \left[ \sum_{i=1}^{N_f} A_{ii} \dot{r}_i(t)^2 + 2 \sum_{i=1}^{N_f} \sum_{j=1}^{N\varphi} B_{ij} \dot{r}_i(t) \dot{s}_j(t) + \sum_{j=1}^{N_\varphi} C_{jj} \dot{s}_j(t)^2 \right], \tag{6}$$

where

$$\begin{cases} A_{ii} = \int_0^{l/2} m(y) f_i(y)^2 dy \\ B_{ij} = -\int_0^{l/2} m(y) \sigma(y) f_i(y) \varphi_j(y) dy \\ C_{jj} = \int_0^{l/2} I_m(y) \varphi_j(y)^2 dy \end{cases}. \tag{7}$$

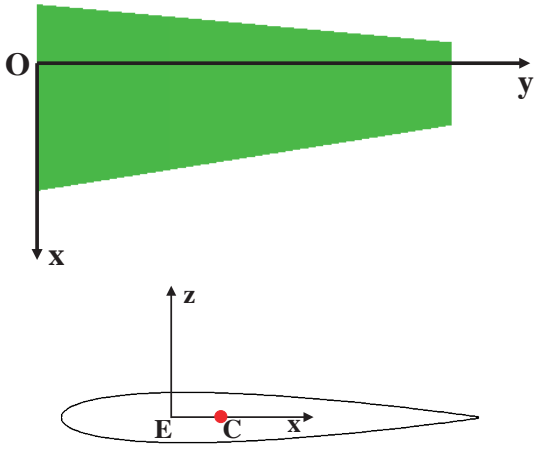


Fig. 7. Wing-fixed coordinate system

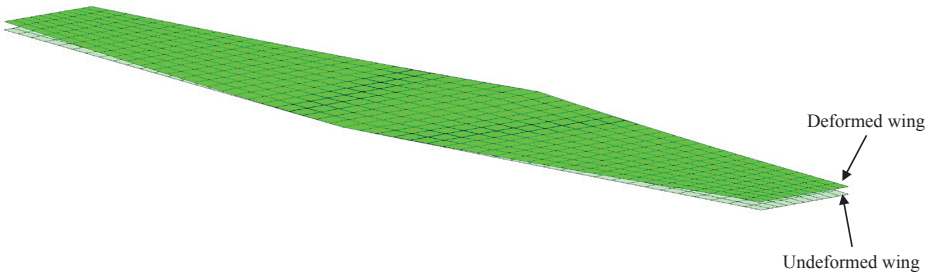


Fig. 6. Wing deformation in trim flight

Here, $m$ and $I_m$ are mass and inertia of moment per unit wing length; $\sigma$ is the coordinate of the center of mass $C$ on the $x$-axis of the wing-fixed coordinate system (Fig. 7).

The strain energy $U$ due to the wing deformations is

$$U = \frac{1}{2}\int_0^{l/2} EI(y)\left(\frac{\partial^2 w_E(y,t)}{\partial y^2}\right)^2 dy + \frac{1}{2}\int_{y=0}^{l/2} GI_p(y)\left(\frac{\partial \theta(y,t)}{\partial y}\right)^2 dy, \quad (8)$$

where $E$ and $I$ are the Young's modulus and the second moment of area of the wing cross section, respectively; $G$ and $I_p$ are the shear modulus and the polar moment of inertia of the wing cross section; $w_E$ and $\theta$ respectively denote the vertical displacement of the elastic center and the rotation angle. The variations of the bending rigidity $EI$ and the torsional rigidity $GI_p$ along the wing span are provided by Bisplinghoff et al [19].

By substituting equation (4) into equation (8), and using the orthogonality of the mode shape functions, we can derive the following expression for the strain energy $U$:

$$U = \frac{1}{2}\sum_{i=1}^{N_f} D_{ii} r_i(t)^2 + \frac{1}{2}\sum_{j=1}^{N_\varphi} E_{jj} s_j(t)^2, \quad (9)$$

where

$$\begin{cases} D_{ii} = \int_0^{l/2} EI(y)\left(\frac{\partial^2 f_i(y)}{\partial y^2}\right)^2 dy \\ E_{jj} = \int_0^{l/2} GI_p(y)\left(\frac{\partial \varphi_j(y)}{\partial y}\right)^2 dy \end{cases}. \quad (10)$$

Generalized forces $Q_i^f$ and $Q_j^\varphi$ associated with the generalized coordinates ri and sj due to aerodynamic loads are

$$\begin{cases} Q_i^f = \sum_{k=1}^{N_p} F_k f_i(y_k) \\ Q_j^\varphi = \sum_{k=1}^{N_p} -F_k x_k \varphi_j(y_k) \end{cases}. \quad (11)$$

In this equation, $N_p$ denotes the total number of aerodynamic panels; $F_k$ is the aerodynamic force acting on the $k^{th}$ panel; $x_k$ and $y_k$ are the coordinates of the $k^{th}$ panel's collocation point on the $x$ and $y$ axes, respectively.

By applying the Lagrange's equation of the second kind [27] along with the expressions from equations (6), (9) and (11), we can derive

$$\mathbf{M}\ddot{\mathbf{q}} + \mathbf{K}\mathbf{q} = \mathbf{Q}, \quad (12)$$

where $\mathbf{M}$ and $\mathbf{K}$ are generalized mass and stiffness matrices, $\mathbf{Q}$ and $\mathbf{q}$ are the vectors of the generalized forces and coordinates, respectively. The expressions of these matrices and vectors are given by equations (13)-(16):

$$\mathbf{M} = \begin{bmatrix} A_{11} & 0 & \cdots & 0 & B_{11} & B_{12} & \cdots & B_{1N_\varphi} \\ 0 & A_{22} & \cdots & 0 & B_{21} & B_{22} & \cdots & B_{2N_\varphi} \\ \vdots & \vdots & \ddots & \vdots & \vdots & \vdots & \vdots & \vdots \\ 0 & 0 & 0 & A_{N_fN_f} & B_{N_f1} & B_{N_f2} & \cdots & B_{N_fN_\varphi} \\ B_{11} & B_{21} & \cdots & B_{N_f1} & C_{11} & 0 & \cdots & 0 \\ B_{12} & B_{22} & \cdots & B_{N_f2} & 0 & C_{22} & \cdots & 0 \\ \vdots & \vdots & \vdots & \vdots & \vdots & \vdots & \ddots & \vdots \\ B_{1N_\varphi} & B_{2N_\varphi} & \cdots & B_{N_fN_\varphi} & 0 & 0 & 0 & C_{N_\varphi N_\varphi} \end{bmatrix}, \quad (13)$$

$$\mathbf{K} = \begin{bmatrix} D_{11} & 0 & \cdots & 0 & 0 & 0 & \cdots & 0 \\ 0 & D_{22} & \cdots & 0 & 0 & 0 & \cdots & 0 \\ \vdots & \vdots & \ddots & \vdots & \vdots & \vdots & \vdots & \vdots \\ 0 & 0 & 0 & D_{N_fN_f} & 0 & 0 & \cdots & 0 \\ 0 & 0 & \cdots & 0 & E_{11} & 0 & \cdots & 0 \\ 0 & 0 & \cdots & 0 & 0 & E_{22} & \cdots & 0 \\ \vdots & \vdots & \vdots & \vdots & \vdots & \vdots & \ddots & \vdots \\ 0 & 0 & \cdots & 0 & 0 & 0 & 0 & E_{N_\varphi N_\varphi} \end{bmatrix}, \quad (14)$$

$$\mathbf{Q} = \begin{bmatrix} Q_1^f & Q_2^f & \cdots & Q_{N_f}^f & Q_1^\varphi & Q_2^\varphi & \cdots & Q_{N_\varphi}^\varphi \end{bmatrix}^T, \quad (15)$$

$$\mathbf{q} = \begin{bmatrix} r_1 & r_2 & \cdots & r_{N_f} & s_1 & s_2 & \cdots & s_{N_\varphi} \end{bmatrix}^T. \quad (16)$$

Equation (12) will be solved numerically using the central finite difference scheme with the second-order accuracy [28].

## 2.5 Artificial Neural Network Model

To predict the responses of the wing structure to random atmospheric turbulence, a recurrent ANN with an external input is used. The turbulence velocity v and the generalized coordinate **q** are the input and the output of the network,

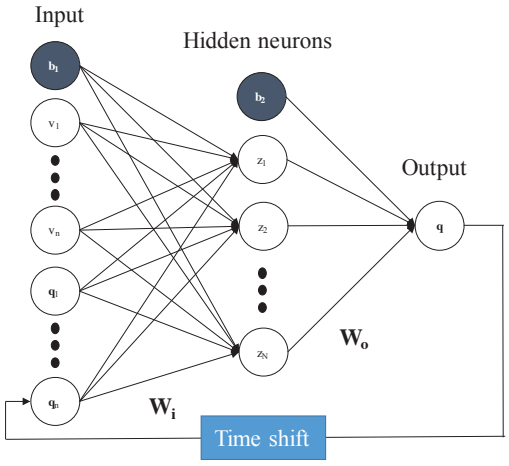


Fig. 8. Structure of artificial neural network

respectively. The network is developed in *MATLAB* software [29], and its layout is sketched in Fig. 8. Here, the input layer of the network includes a bias $\mathbf{b}_1$ together with the time series of the turbulence velocity $v_1$, $v_2$, ..., $v_n$ and the generalized coordinates $\mathbf{q}_1$, $\mathbf{q}_2$, ..., $\mathbf{q}_n$ from the recent $n$ time steps. The hidden layer comprises a bias $\mathbf{b}_2$ and 50 neurons $z_1$, $z_2$, ..., $z_{50}$. Biases can be perceived as "extra" neurons that are added to each layer and not connected to any previous layer. The introduction of biases allows us to shift transfer functions left or right flexibly, then the training process becomes more effective. The network predicts the current value of the generalized coordinate $\mathbf{q}$, which is fed back to become an input $\mathbf{q}_n$ for the next prediction. The value of the delay number $n$ may have a significant influence on the quality of prediction results, and the selection of $n$ will be discussed in the following section. Sigmoid and linear transfer functions are respectively used in the hidden and the output layers. The input and the hidden layers, as well as the hidden and the output layers are connected to each other by the sets of weights $\mathbf{W}_i$ and $\mathbf{W}_o$, respectively.

For the training process, data are randomly divided with 70% used for training and 30% for testing. The network utilizes the Bayesian regularization backpropagation that updates the weights and biases according to the Levenberg-Marquardt optimization method [29,30]:

$$\mathbf{W}_{k+1} = \mathbf{W}_k - \left(\mathbf{J}^T\mathbf{J} + \mu\mathbf{I}\right)^{-1}\mathbf{J}^T\mathbf{e}, \tag{17}$$

where $\mathbf{W}$ is a vector that contains all the weights and biases; $\mathbf{J}$ is the Jacobian matrix consisting of the first derivatives of network errors with respect to the weights and biases; $\mathbf{e}$ is a vector of network errors; $\mathbf{I}$ is a unit matrix; and $\mu$ is a learning step size parameter, whose value decreases after each successful step. The use of the Bayesian regularization, which minimizes a linear combination of squared errors and weights, can assure a better solution for noisy problems. More details about the Bayesian regularization can be found in [31].

## 3. Results and Discussion

The ANN depicted in Fig. 8 is trained to predict the dynamic responses of the wing structure. The values of the weights and biases are updated during the training process by equation (17). For this process, the program uses data related to the turbulence profile shown in Fig. 1, and its corresponding solution (generalized coordinate vector $\mathbf{q}$) obtained by numerically solving the dynamic equation (12). The time histories of the generalized coordinates used for the training are shown in Fig. 9. Fig. 10 shows the wake visualization when the airplane is encountering atmospheric turbulence.

As mentioned earlier, the number of time delay $n$ is of great importance in our ANN; thus, it is necessary to choose a proper value that can give a compromise between accuracy and computational complexity. Prediction errors corresponding to the time delay number $n$ varying from 5 to 30 are investigated. In this task, turbulence profiles used for the training and prediction processes have the RMS gust velocity $\sigma_w$ of 6 m/s, and the durations of these profiles are 20 and 45 seconds, respectively. The effects of the time delay number n on the prediction errors of the bending and torsional moments are shown in Fig. 11. In this figure, the quality of the predictions is indicated through the relative errors of the bending and torsional moments at the wing

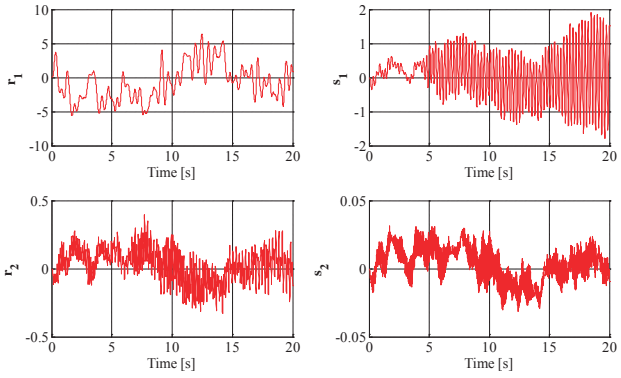


Fig. 9. Data of the generalized coordinates used for training

Fig. 10. Wake visualization during flight

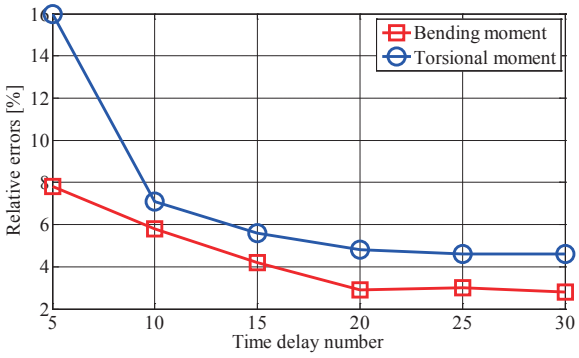


Fig. 11. Relative errors of bending and torsional moments against the time delay number $n$

root. The relative errors are defined as the ratios of the RMS errors to the RMS moments. The exact bending and torsional moments are obtained by solving equation (12) numerically. It should be noted that the values of the moments in the trim condition are excluded from the results.

It is observed that the prediction becomes more accurate as the number of time delay $n$ increases. After the value of 20, there is almost no improvement in the prediction results. The number of time delay is associated with the length of the free wake involved in the computation. When $n$ equals 20, this length is about 1.5 times of the wing span. With a lower value of n, the wake included in the computation becomes shorter; therefore, the result is less accurate due to the insufficiency of the wake information. Considering the compromise between the accuracy of the prediction and the complexity of the training process, $n$ is set to 20 for the present problem.

Using the time delay number $n$ of 20, the validity of the ANN is tested against the variation of the RMS gust velocity $\sigma_w$. Various different turbulence profiles with a duration of 45 seconds and $\sigma_w$ varying from 2 m/s to 8 m/s are generated and shown in Fig. 12. The value of $\sigma_w$ from 2 m/s to 8 m/s can represent various levels of turbulence intensity ranging from light turbulence to extremely severe one [32]. Fig. 13 exhibits the time histories of predicted and exact bending and torsional moments along with their errors.

From Fig. 13 and Table 1, it is seen that the ANN can

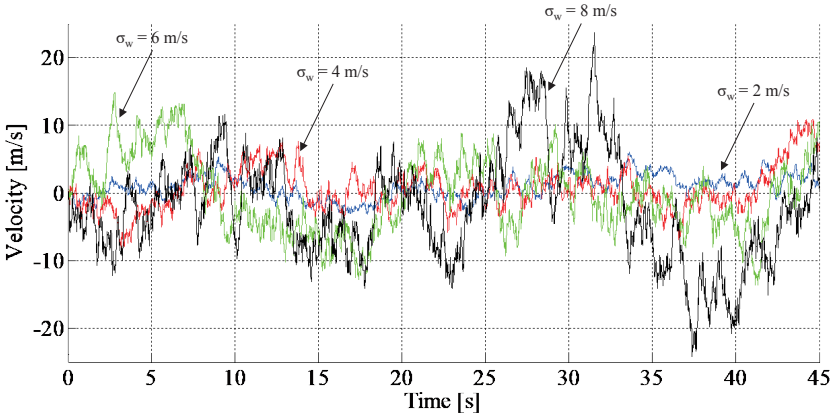


Fig. 12. Random atmospheric turbulence velocity profiles with various values of RMS gust velocity $\sigma_w$

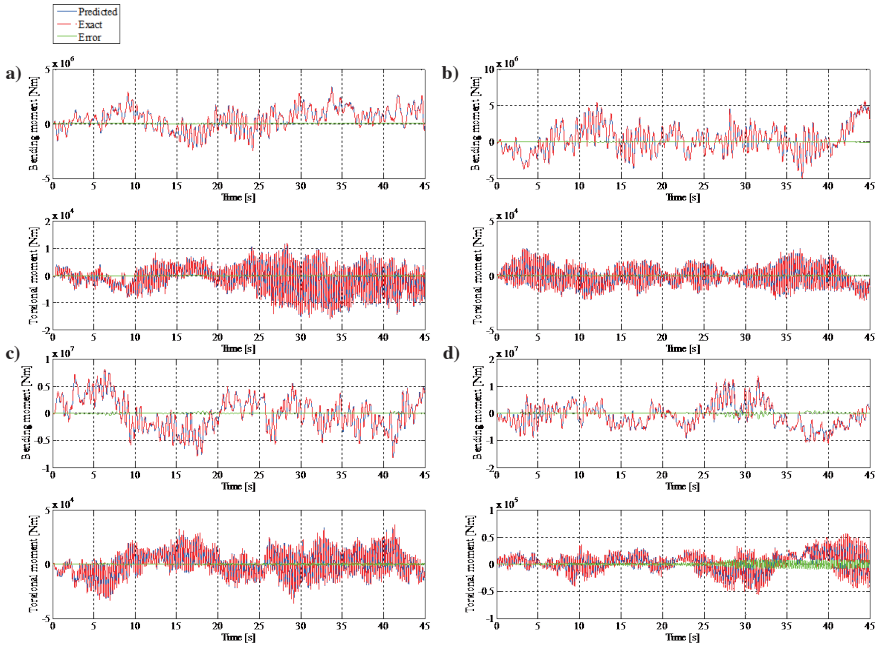


Fig. 13. Bending and torsional moments due to atmospheric turbulence with various values of RMS gust velocity σw: a) $\sigma_w$=2 m/s; b) $\sigma_w$=4 m/s; c) $\sigma_w$=6 m/s; d) $\sigma_w$=8 m/s

predict structural dynamic responses due to atmospheric turbulence with a high level of accuracy. Particularly, the computational time is reduced dramatically with the use of the ANN. Using the conventional way to estimate structural dynamic responses due to atmospheric turbulence, equation (12) has to be solved numerically. Thus, the program is required to update the wake geometry and compute the aerodynamic pressure distribution after each time step. This process demands a great computational resource to store all of the information related to the history of the wake. To obtain the results corresponding to a 45-second turbulence profile with the implementation of a parallel computing technique, a computer using an eight-thread processor has to run about one hour. When the ANN approach is applied, the equation (12) is required to be solved only once for a relatively short-duration turbulence profile (20 seconds) to obtain the training data. Once the network has been trained, it can be applied for any other longer-duration atmospheric turbulence profile. Moreover, instead of running a lengthy solving process as that of the conventional approach, the ANN can provide the predicted results instantaneously.

As shown in Fig. 13 and Table 1, when the RMS gust velocity $\sigma_w$ ranges from 2 m/s to 6 m/s, the ANN can predict the dynamic responses of the wing structure due to atmospheric turbulence with small errors that are below 5%. However, when $\sigma_w$ equals 8 m/s, prediction errors could be over 10%. It is due to the fact that the training data used in this study are from a turbulence profile with $\sigma_w$ of 6 m/s (Fig. 1). For a more severe atmospheric turbulence profile, there may exist some intervals of time, in which the velocity is higher than that from the training data (Fig. 12). In other words, the machine has not been trained to properly deal with these high velocity cases; hence, some noticeable errors could occur. However, turbulence with $\sigma_w$=8 m/s is regarded as an extremely severe case that may happen only once in about $5\times10^5$ flight hours [32]. Moreover, it is also found that the prediction results of the bending moment by the ANN is generally more precise than those of the torsional moment. This finding can be explained by the higher natural frequencies of the torsional modes (Fig. 2), which make torsional vibrations noisier, and therefore, more difficult to predict than bending vibrations.

Table 1. Relative errors of bending and torsional moments. $\sigma_f$ and $\sigma_p$ are RMS values of bending and torsional moments; $\sigma_f^e$ and $\sigma_p^e$ are their RMS errors.

| $\sigma_w$ (m/s) | $\sigma_f^e/\sigma_f$ (%) | $\sigma_p^e/\sigma_p$ (%) |
|---|---|---|
| 2 | 1.3 | 1.7 |
| 4 | 1.2 | 1.9 |
| 6 | 2.9 | 4.8 |
| 8 | 7.3 | 19.8 |

The prediction errors of the generalized coordinates $r_1$, $r_2$, $s_1$ and $s_2$ are also estimated and shown in Table 2. By comparing the values in Tables 1 and 2, it is found that the errors of the bending and torsional moments are substantially associated with those of the generalized coordinates $r_1$ and $s_1$, which are corresponding to the first bending and torsional modes, respectively.

For the next analysis, the effect of the scale of turbulence $L_s$ on the accuracy of the prediction is studied. Together with the case of $L_s$ equal to 762 m, the errors in two other cases corresponding to $L_s$ of 508 m and 1143 m are calculated and given in Table 3. Here, the RMS gust velocity $\sigma_w$ is 6 m/s.

It is easy to recognize that the errors tend to grow as the scale of turbulence decreases. When studying the variation of the velocity PSD curve in Fig. 14, it is found that atmospheric

Table 3. Relative errors of bending and torsional moments against the scale of turbulence $L_s$.

| $L_s$ (m) | $\sigma_f^e/\sigma_f$ (%) | $\sigma_p^e/\sigma_p$ (%) |
|---|---|---|
| 508 | 4.1 | 9.7 |
| 762 | 2.9 | 4.8 |
| 1143 | 2.1 | 2.6 |

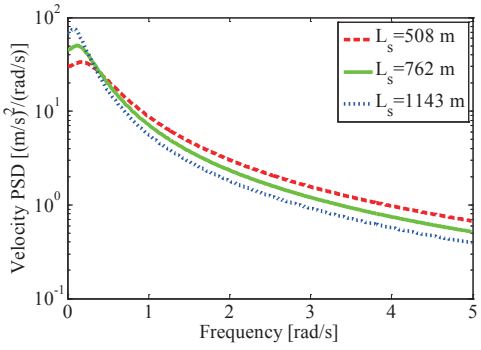


Fig. 14. Velocity PSD curve against the scale of turbulence $L_s$

Table 2. Relative errors of generalized coordinates $r_1$, $r_2$, $s_1$ and $s_2$.

| $\sigma_w$ (m/s) | $\sigma_{r_1}^e/\sigma_{r_1}$ (%) | $\sigma_{r_2}^e/\sigma_{r_2}$ (%) | $\sigma_{s_1}^e/\sigma_{s_1}$ (%) | $\sigma_{s_2}^e/\sigma_{s_2}$ (%) |
|---|---|---|---|---|
| 2 | 1.3 | 3.7 | 1.7 | 9.0 |
| 4 | 1.2 | 2.1 | 1.9 | 4.8 |
| 6 | 3.1 | 1.7 | 4.7 | 4.5 |
| 8 | 7.8 | 7.8 | 19.6 | 10.7 |

turbulence with a lower $L_s$ has greater power distributed in a high frequency range. Consequently, a lower scale of turbulence will result in a noisier input, and thus, a lower level of prediction accuracy.

Finally, to confirm the applicability of the ANN approach for gust response prediction problems, results corresponding to other values of flight speed $V$ are obtained. In fact, when the flight speed is changed, the trim condition has to be found again. In addition, the ANN is reconstructed and trained. The number of time delay $n$ is altered accordingly so that the length of the wake included in the computation is about 1.5 times of the wing span. Thus far, we have studied only the case corresponding to the flight speed $V$ of 700 km/h. When $V$ is changed to 630 km/h and 770 km/h, the relative errors of the bending moment are 3.6% and 1.7%, and those of the torsional moment equal 5.2% and 8.1%, respectively. In general, these errors are relatively small and acceptable for gust response prediction tasks.

## 4. Conclusions

This paper has presented an alternative low-cost model based on artificial neural networks (ANNs) to predict the dynamic responses of a wing structure due to random atmospheric turbulence in the time domain. The wing structure is simplified by a classical beam, and the nonlinear unsteady vortex-lattice method is applied to compute the pressure distribution. The angle of attack and the deformed shape of the wing in the trim condition were achieved by an iterative method. The Lagrange's equation of the second kind was used to derive the governing equations for the structural dynamics problem. In this study, a recurrent ANN was developed and trained based on data obtained from a turbulence profile with a root-mean-square gust velocity of 6 m/s. The validity of the ANN was confirmed for various different cases of long-duration turbulence. When the ANN is used, instead of running a numerical program for hours, the accurate results of the wing structure' dynamic responses due to atmospheric turbulence could be obtained instantaneously. The results also showed that when the ANN is applied to a turbulence model with a higher root-mean-square gust velocity than that of the training data, there could be some errors that are explained by the existence of high velocity intervals. Predictions by the ANN for bending moments, whose vibrations occur at lower frequencies, appear to be more precise than those for torsional moments. Similarly, for atmospheric turbulence with a larger scale of turbulence $L_s$, the ANN can produce a better prediction result. Moreover, the validity of the current approach was also confirmed with respect to several values of flight speed. In general, in most cases, the relative errors of the bending and torsional moments are lower than 5%; thus, it can be concluded that using ANNs is an efficient, high-fidelity alternative method for the problems of gust response predictions.

## Acknowledgement

This work was supported by the Technology Innovation Program (10074278, Development of a SHM system for UAV using CNT/Polymer hybrid fiber sensor network and simultaneous proof-of-concept of autonomous flight and diagnosis) funded By the Ministry of Trade, industry & Energy (MI, Korea)

## References

[1] Wilson, E. B., "Theory of an Aeroplane Encountering Gusts", *Proceedings of the National Academy of Sciences*, Vol. 2, No. 5, 1916, pp. 294-297.

[2] Etkin, B., "A Theory of the Response of Airplanes to Random Atmospheric Turbulence", *Journal of the Aerospace Sciences*, Vol. 26, No. 7, 1959, pp. 409-420. DOI: 10.2514/8.8127

[3] Regulations, F. A., "Part 25-Airworthiness Standards: Transport Category Airplanes", *Federal Aviation Administration (FAA), USA*, 1970.

[4] "Certification Specifications for Large Aeroplanes CS-25", *European Aviation Safety Agency*, 2008.

[5] Hoblit, F. M., *Gust Loads on Aircraft: Concepts and Applications*, AIAA Education Series, 1988.

[6] Beal, T. R., "Digital Simulation of Atmospheric Turbulence for Dryden and Von Karman Models", *Journal of Guidance, Control, and Dynamics*, Vol. 16, No. 1, 1993, pp. 132-138. DOI: 10.2514/3.11437

[7] Zhenxing, G. and Hongbin, G., "Generation and Application of Spatial Atmospheric Turbulence Field in Flight Simulation", *Chinese Journal of Aeronautics*, Vol. 22, No. 1, 2009, pp. 9-17. DOI: 10.1016/S1000-9361(08)60063-1

[8] Kanda, A. and Dowell, E. H., "Worst-Case Gust-Response Analysis for Typical Airfoil Section with Control Surface", *Journal of Aircraft*, Vol. 42, No. 4, 2005, pp. 956-962. DOI: 10.2514/1.8931

[9] Khodaparast, H. H. and Cooper, J. E., "Rapid Prediction of Worst-Case Gust Loads Following Structural Modification", *AIAA Journal,* Vol. 52, No. 2, 2014, pp. 242-254. DOI: 10.2514/1.J052031

[10] Wang, Z., Chen, P. C., Liu, D. D. and Mook, D. T.,

"Nonlinear-Aerodynamics/Nonlinear-Structure Interaction Methodology for a High-Altitude Long-Endurance Wing", *Journal of Aircraft*, Vol. 47, No. 2, 2010, pp. 556-566. DOI: 10.2514/1.45694

[11] Raveh, D. E., "CFD-Based Models of Aerodynamic Gust Response", *Journal of Aircraft*, Vol. 44, No. 3, 2007, pp. 888-897. DOI: 10.2514/1.25498

[12] Albano, E., "A Doublet-Lattice Method for Calculating Lift Distributions on Oscillating Surfaces in Subsonic Flows", *AIAA Journal*, Vol. 7, No. 2, 1969, pp. 279-285.

[13] Eversman, W. and Tewari, A., "Consistent Rational Fraction Approximation for Unsteady Aerodynamics", *Journal of Aircraft*, Vol. 28, No. 9, 1991, pp. 545-552. DOI: 10.2514/3.46062

[14] Peng, W., Zhang, J. and You, L., "The Hybrid Uncertain Neural Network Method for Mechanical Reliability Analysis", *International Journal of Aeronautical and Space Sciences*, Vol. 16, No. 4, 2015, 510-519. DOI: 10.5139/IJASS.2015.16.4.510

[15] Wan, Z., Wang, X. and Yang, C., "A Highly Efficient Aeroelastic Optimization Method Based on a Surrogate Model", *International Journal of Aeronautical and Space Sciences*, Vol. 17, No. 4, 2016, pp. 491-500. DOI: 10.5139/IJASS.2016.17.4.491

[16] Yao, W. and Liou, M. S., "Reduced-Order Modeling for Flutter/LCO Using Recurrent Artificial Neural Network", *12th AIAA Aviation Technology, Integration, and Operations (ATIO) Conference and 14th AIAA/ISSMO Multidisciplinary Analysis and Optimization Conference*, Indianapolis, Indiana, 2012.

[17] Mannarino, A. and Mantegazza, P., "Nonlinear Aeroelastic Reduced Order Modeling by Recurrent Neural Networks", *Journal of Fluids and Structures*, Vol. 48, 2014, pp. 103-121. DOI: 10.1016/j.jfluidstructs.2014.02.016

[18] Ly, U. L. and Chan, Y. K., "Time-Domain Computation of Aircraft Gust Covariance Matrices", *6th Atmospheric Flight Mechanics Conference, Guidance, Navigation, and Control and Co-located Conferences*, Danvers, MA, 1980.

[19] Bisplinghoff, R. L., Ashley, H. and Halfman, R. L., *Aeroelasticity*, Dover Publications Inc., New York, 1955.

[20] Kwon, Y. W. and Bang, H., *The Finite Element Method Using MATLAB*, CRC Press, New York, 2000.

[21] Nguyen, A. T. and Han, J., "Simulation and Analyses of Dynamic Gust Responses of a Flexible Aircraft Wing Under Continuous Random Atmospheric Turbulence", *16th Asia Pacific Vibration Conference*, Hanoi, Vietnam, 2016.

[22] Katz, J. and Plotkin, A., *Low-Speed Aerodynamics: From Wing Theory to Panel Methods*, Cambridge University Press, 2001.

[23] Nguyen, A. T., Kim, J. K., Han, J. S. and Han, J. H., "Extended Unsteady Vortex-Lattice Method for Insect Flapping Wings", *Journal of Aircraft*, Vol. 53, No. 6, 2016, pp. 1709-1718. DOI: 10.2514/1.C033456

[24] Nguyen, A. T., Han, J. S. and Han, J. H., "Effect of Body Aerodynamics on the Dynamic Flight Stability of the Hawkmoth Manduca Sexta", *Bioinspiration & Biomimetics*, Vol. 12, No. 1, 2017, p. 016007. DOI: 10.1088/1748-3190/12/1/016007

[25] Willis, D. J., Peraire, J. and White, J. K., "A Combined pFFT-Multipole Tree Code, Unsteady Panel Method with Vortex Particle Wakes", *International Journal for Numerical Methods in Fluids*, Vol. 53, No. 8, 2007, pp. 1399-1422. DOI: 10.1002/fld.1240

[26] Jian, Z. and Jinwu, X., "Nonlinear Aeroelastic Response of High-Aspect-Ratio Flexible Wings", *Chinese Journal of Aeronautics*, Vol. 22, No. 4, 2009, pp. 355-363. DOI: 10.1016/S1000-9361(08)60111-9

[27] Craig, R. R. and Kurdila, A. J., *Fundamentals of Structural Dynamics*, John Wiley & Sons, 2006.

[28] Lynch, D. R., *Numerical Partial Differential Equations for Environmental Scientists and Engineers: A First Practical Course*, Springer, 2004.

[29] Beale, M. H., Hagan, M. T. and Demuth, H. B., *Neural Network Toolbox™ User's Guide*, The Math Works, Inc., 2012.

[30] Marquardt, D. W., "An Algorithm for Least-Squares Estimation of Nonlinear Parameters", *Journal of the Society for Industrial and Applied Mathematics*, Vol. 11, No. 2, 1963, pp. 431-441. DOI: 10.1137/0111030

[31] MacKay, D. J. C., "Bayesian Interpolation", *Neural Computation*, Vol. 4, No. 3, 1992, pp. 415-447. DOI: 10.1162/neco.1992.4.3.415

[32] "Flying Qualities of Piloted Aircraft MIL-STD-1797", Department of Defense, 1997.